

## Accepted Manuscript

Eulerian description of non-stationary motion of an idealized belt-pulley system with dry friction

Evgenii Oborin, Yury Vetyukov, Ivo Steinbrecher

PII: S0020-7683(18)30151-3  
DOI: [10.1016/j.ijsolstr.2018.04.007](https://doi.org/10.1016/j.ijsolstr.2018.04.007)  
Reference: SAS 9962



To appear in: *International Journal of Solids and Structures*

Received date: 6 October 2017  
Revised date: 13 March 2018  
Accepted date: 7 April 2018

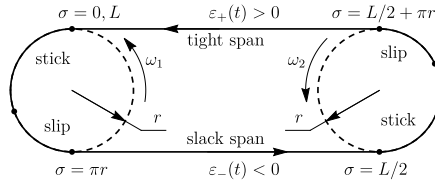
Please cite this article as: Evgenii Oborin, Yury Vetyukov, Ivo Steinbrecher, Eulerian description of non-stationary motion of an idealized belt-pulley system with dry friction, *International Journal of Solids and Structures* (2018), doi: [10.1016/j.ijsolstr.2018.04.007](https://doi.org/10.1016/j.ijsolstr.2018.04.007)

This is a PDF file of an unedited manuscript that has been accepted for publication. As a service to our customers we are providing this early version of the manuscript. The manuscript will undergo copyediting, typesetting, and review of the resulting proof before it is published in its final form. Please note that during the production process errors may be discovered which could affect the content, and all legal disclaimers that apply to the journal pertain.

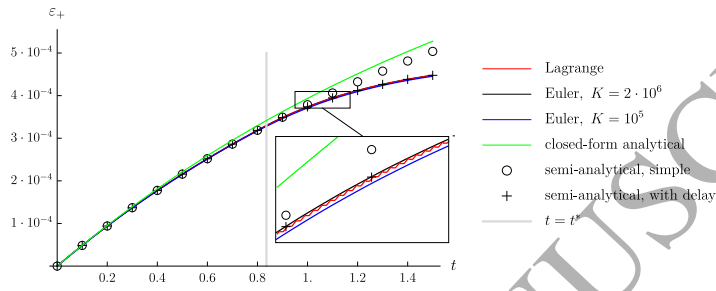
**Highlights**

- Mathematical model of a belt drive with dry friction at Eulerian description
- Novel non-material finite element implementation with stick and slip effects
- Novel analytical result for the time evolution of the slip zones in a belt drive
- Justified by analytics, non-material FE is ready for practically relevant problems

### Graphical Abstract



Time variation of the strain in the tight span, analytical and FEM solutions



# Eulerian description of non-stationary motion of an idealized belt-pulley system with dry friction

Evgenii Oborin<sup>a,\*</sup>, Yury Vetyukov<sup>b</sup>, Ivo Steinbrecher<sup>a</sup>

<sup>a</sup>*Johannes Kepler University Linz, Altenbergerstraße 69, A-4040 Linz, Austria*

<sup>b</sup>*Vienna University of Technology, Getreidemarkt 9, A-1060 Vienna, Austria*

---

## Abstract

We develop and validate a mathematical model of a belt drive with dry friction between the belt and the pulleys. Considering an idealized setting, we make use of the Eulerian (spatial) kinematic description for the belt, which moves quasistatically along a given contour. The focus of the paper lies on modelling the friction law in a non-material finite element framework. We also obtained a novel analytical result for the time evolution of the zones of sliding friction and stick. The correspondence of the analytical solution to both the non-material and conventional material finite element simulations has been demonstrated.

*Keywords:* Belt drive mechanics, Eulerian description, Finite element analysis, Dry friction, Contact problem

*2010 MSC:* 74K05, 74M10, 74S05, 70-08, 74G05, 35Q74

---

## 1. Introduction

Belonging formally to the field of mechanics of solids, the problem of mathematical modelling of a belt drive has similarities to fluid mechanics. The interest is usually focused on the time history of mechanical fields in a particular point in space rather than on following them in a given material point of the belt, which permanently enters and leaves the domains of contact with the pulleys.

---

\*Corresponding author

*Email addresses:* [evgenii.oborin@jku.at](mailto:evgenii.oborin@jku.at) (Evgenii Oborin),  
[yury.vetyukov@tuwien.ac.at](mailto:yury.vetyukov@tuwien.ac.at) (Yury Vetyukov), [ivo.steinbrecher@jku.at](mailto:ivo.steinbrecher@jku.at) (Ivo Steinbrecher)

This is generally typical for axially moving structures, which have been extensively treated in the literature; here we mention the classical linear analysis by Mote (1966) and Wickert (1992) as well as the works (Steinbrecher et al., 2017; Saksa et al., 2012; Kurki et al., 2016). It has long been established, that Lagrangian (material) kinematic description is not an optimal choice for this sort of problems, in particular for numerical methods with spatial discretization, see discussion in Sect. 3 below. Purely Eulerian (spatial) (Eliseev and Vetyukov, 2012; Vetyukov et al., 2017b) or mixed Eulerian-Lagrangian (Vetyukov et al., 2016, 2017a) formulations are advantageous as we discretize the problem in a domain-specific manner and avoid the so-called variational crime because of imposing contact conditions on a part of a single finite element.

Eliseev and Vetyukov (2012) and Vetyukov et al. (2017b) have applied the Eulerian description to modelling transient dynamics of belt drives under the assumption of an idealized point contact based on the original formulation by Eliseev (2009). Exact solutions of the problem of an extensible belt moving between the pulleys with dry friction law of contact were provided by Rubin (2000), Bechtel et al. (2000), Morimoto and Iizuka (2012) for stationary regimes of motion. Leamy (2005) as well as Kim et al. (2011) considered perturbations of stationary motion, which should allow studying transient regimes with sufficiently small and slow deviations from a given steady one. Hong and Ren (2011) suggested a mixed finite element formulation, which combines Lagrangian nodes with Arbitrary Lagrangian-Eulerian ones using constraint conditions, typical for Multibody Systems Dynamics, and which can theoretically be applied to the considered class of problems. Large vibrations of an axially moving string were treated geometrically exact in a mixed Eulerian-Lagrangian finite element framework using Lagrange's equations of motion of the second kind by Vetyukov (2018). Denoël and Detournay (2011) proposed semi-analytical schemes of the analysis of a three-dimensional elastica constrained in a channel in terms of an Eulerian curvilinear coordinate along the axis of the channel.

Here we aim at developing and validating a mathematical model of dry friction contact at non-material description. The frictional contact of elastic

bodies is a subject of both analytical and experimental investigations because of its responsibility for the effects of belt creep, micro-slip and so-called frictional ratcheting, see (Wetter and Popov, 2014; Mojdehi et al., 2017; Yastrebov, 2013). We intend to resolve the time evolution of the domains of stick and slip in the contact region in the framework of the transient quasistatic analysis neglecting the effect of inertia. The considered idealized quasistatic formulation with no transverse motion of the belt serves as a "sandbox" for testing the numerical scheme and comparing it to a semi-analytical solution of the derived system of delay differential equations. To the best knowledge of the authors, both the Eulerian finite element formulation with dry friction law as well as the analytical solution are novel results, which were not previously published in the open literature. The approach is intended to become a corner-stone of a further sophisticated analysis with

- transverse action of the field of gravity,
- imperfect geometries of the pulleys,
- time-varying contact domains because of the transverse deflections of the belt,
- string, beam or shell model of the belt (Belyaev et al., 2017).

## 2. Statement of the problem and qualitative analysis

As depicted in Fig. 1, we consider a belt drive with two equal pulleys and an extensible belt, which moves counter-clockwise along a given trajectory with an arc coordinate  $\sigma$ . The length of the looped contour is  $L$  and the coordinates  $\sigma = 0$  and  $\sigma = L$  both correspond to the point, where the belt comes into contact with the left (*driving*) pulley rotating with the angular velocity  $\omega_1$ . The *driven* (right) pulley rotates slower,  $\omega_2 < \omega_1$ ; both angular velocities are taken as kinematically prescribed for simplicity. With  $r$  being the radius of both pulleys, we divide the domain into two *contact regions*

$$0 \leq \sigma \leq \pi r, \quad L/2 \leq \sigma \leq L/2 + \pi r \quad (1)$$

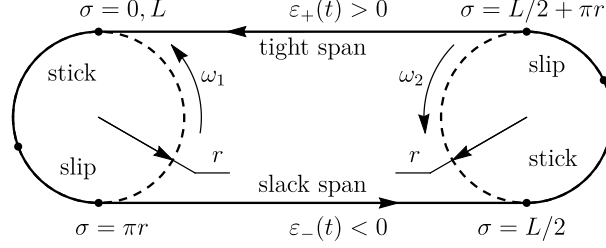


Figure 1: Belt on two rotating pulleys: contour motion

and two free spans: the *tight* one,

$$L/2 + \pi r < \sigma < L, \quad (2)$$

in which the tension of the belt is higher, and the *slack* one,

$$\pi r < \sigma < L/2, \quad (3)$$

with lower tension. The present research aims at a methodology to model the dry friction contact between the belt and the pulley at a non-material kinematic description and to validate it against analytical and other numerical solutions. We are focusing at the case of moderately large slipping zones compared to the size of the contact regions, but do not consider the situation when the belt is sliding everywhere. This goal is achieved by using an idealized model with the following assumptions.

- Considering a *quasistatic* process, we neglect the inertia of the belt, but investigate the time evolution of the system seeking an equilibrium path when the pulleys rotate.
- Neglecting the bending stiffness of the belt and the transverse loadings, we restrict the analysis to the case of *contour motion* of an extensible string with known boundaries of the contact regions.
- We assume the initial pre-stretch and the pre-tension of the belt to be high compared to their variations because of the deformation. This means

that the normal contact force, which is determined by the tension and the curvature, remains constant. The tangent *force of sliding friction*  $f$  (which is also the maximal sticking contact force) becomes now a given parameter of the problem and is known in advance.

Transient dynamics of the belt at contour motion was studied by the authors in (Vetyukov et al., 2017b) under the assumption of an idealized contact model with the zone of sliding friction degenerated into a point. The entire complexity of the dry friction process along with the inertial effects were taken into account by Rubin (2000) and by Bechtel et al. (2000), whose analysis was restricted to the stationary motion of the system. The present study of the transient motion with the time evolution of the dry friction process could not be found in the open literature and thus appears to be new.

The high initial pre-tension of the belt is balanced by the constant normal contact forces. The entire analysis below features just the presumably small *variations* of the strain of the belt and of the tension force from the initial values. We focus on modelling friction and leave the complicated nonlinear effects because of the high initial pre-stretch for the future work. Denoting the variation of the strain (simply strain in the following) by  $\varepsilon$  and the variation of the tension force by  $Q$ , we write a linear constitutive relation with the tension stiffness  $b$ :

$$Q = b\varepsilon. \quad (4)$$

The pulleys begin rotating at the time  $t = 0$ , when there is no strain in the belt,

$$\varepsilon|_{t=0} = 0. \quad (5)$$

Now both contact regions are entirely in the *stick mode*, but the particles at the driving pulley move faster as  $\omega_1 > \omega_2$ . More particles enter the slack span per time unit than leave it, and more particles leave the tight span than enter it: the strain  $\varepsilon_+$  at the tight span starts growing, while the strain  $\varepsilon_-$  at the slack one decreases. The contact regions are primarily undeformed, but the parts of the belt with non-zero strains begin entering them from the points



$\sigma = 0$  and  $\sigma = L/2$ . As no jumps in  $Q$  are possible in the points  $\sigma = \pi r$  and  $\sigma = L/2 + \pi r$  at dry friction contact, zones of slip begin to appear and grow along with the magnitudes of  $\varepsilon_+$  and  $\varepsilon_-$ . This effect is known in the literature as *belt creep* and was first studied by Reynolds (1874). While the analysis is simple for a stationary process and is widely discussed in the technical literature, see e.g. (Stolarski, 1990), a transient solution is far more sophisticated. During the initial stage of motion of the system both contact regions are divided in three parts:

1. zones with *stick contact* and  $\varepsilon \neq 0$ , which are adjacent to the entry touching points  $\sigma = 0$  and  $\sigma = L/2$ ,
2. zones with stick contact and  $\varepsilon = 0$  (we shall call them *pre-historic zones*, which are the remainders of the initial undeformed state),
3. zones with *slip contact*, in which the strain varies between 0 and  $\varepsilon_{+,-}$  in the exit touching points  $\sigma = \pi r$  and  $\sigma = L/2 + \pi r$ , respectively.

Later on, the first and the third zones meet each other as the pre-historic zones collapse. The analysis shows, that when the angular velocities are close to each other and the strains are small, this collapse happens nearly simultaneously at both pulleys at a time instant  $t = t^*$ , see the discussion in the end of Sect. 4.1. Just the zone of stick with constant  $\varepsilon$  and the zone of slip with varying  $\varepsilon$  remain in each contact region in the stationary mode, when the difference in material velocities of the pulley surfaces is balanced by different stretches of the belt. The solution is certainly more complicated at time-varying  $\omega_{1,2}$ , see example in Sect. 7.

### 3. Lagrangian finite element solution

We begin with a simple finite element implementation using Lagrangian description of the motion of the belt, see (Dufva et al., 2007; Kubas, 2017) for examples of its usage to the considered kind of problems. Particles of the belt are identified by their material coordinates  $s$ . Their actual position at a given

time  $t$  is determined by the contour coordinate

$$\sigma = \sigma(s, t), \quad \varepsilon = \frac{\partial \sigma}{\partial s} - 1 \equiv \partial_s \sigma - 1, \quad \sigma(s, 0) = s, \quad (6)$$

the material coordinate equals the contour one in the initial state. The velocity of a particle

$$v = \left. \frac{\partial \sigma}{\partial t} \right|_{s=\text{const}} \equiv \dot{\partial}_t \sigma \quad (7)$$

is a material time derivative of the coordinate at constant  $s$ , which we denote by  $\dot{\partial}_t$ .

In a quasistatic formulation we seek an equilibrium by solving the balance equation

$$\partial_s Q + q = 0, \quad (8)$$

the increment of the tension force  $Q$  from a pre-stretched state follows from the linear constitutive law Eq. (4). The force of dry friction  $q$  vanishes in the free spans and equals either  $\pm f$  in the sliding zones or is  $-f \leq q \leq f$  in the zones of stick. Aiming at a finite element implementation, we formulate a mathematically equivalent problem of minimization of the total potential energy of the model, which results from the strain energy of the belt and the potential of contact forces:

$$U[\sigma] = U^{\text{strain}} + U^{\text{contact}} \rightarrow \min, \quad (9)$$

$$U^{\text{strain}} = \int_0^L \frac{1}{2} b \varepsilon^2 ds, \quad U^{\text{contact}} = - \int_0^L q \sigma ds.$$

The quadratic strain energy corresponds to the linear constitutive law Eq. (4). The minimization problem Eq. (9) needs to be accomplished by the knowledge of the current contact state in each point of the belt:

- *no contact* – the current coordinate  $\sigma$  is within one of the two free spans Eq. (2) or Eq. (3),  $q = 0$ ;
- *slip backward* – the material particle is moving slower than the surface of the corresponding pulley,  $v < \omega_{1,2} r$ , and  $q = f$  is the maximal friction force per unit length of the belt, which is determined by the pre-tension;

- *slip forward* – the material particle overtakes the surface of the pulley,  $v > \omega_{1,2}r$ ,  $q = -f$ ;
- *stick* – the material particle is moving together with the pulley,  $v = \omega_{1,2}r$ ,  $-f \leq q \leq f$ .

In the zones of sticking contact, we force the particles moving together with the pulleys by adding the corresponding kinematic constraints to the minimization problem Eq. (9). At each time step we need to check the inequalities for the force  $q$  in order to guarantee the consistency of the solution.

The finite element model makes use of a linear approximation of the unknown function  $\sigma(s, t)$  by the values  $\sigma_i(t)$  in the nodes  $s_i = hi$ , the material length of each finite element  $h = L/n$  is defined by the total number of elements  $n$ . The mesh is looped, which means that the expression for the strain within the  $n$ -th element is treated differently:

$$\varepsilon_i^{\text{el}} = \begin{cases} (\sigma_{i+1} - \sigma_i)/h - 1, & 1 \leq i \leq n-1 \\ (\sigma_1 + L - \sigma_n)/h - 1, & i = n \end{cases} \quad (10)$$

Now the strain energy is a quadratic form of the nodal unknowns  $\sigma_i(t)$ , and the current contact state is attributed to the nodes. Initially we assume stick in the entire contact regions. During the time integration, we resolve the transition conditions between the contact states explicitly. Proceeding to a new time step over the time interval  $\tau$ , we update the solution by performing the following stages.

1. We apply kinematic conditions in the sticking nodes increasing their coordinates  $\sigma_i$  by the values  $\tau\omega_{1,2}r$  and thus promoting the motion of the system.
2. Then we seek an equilibrium minimizing Eq. (9) with respect to the degrees of freedom of the nodes, which are currently sliding or not in contact. The total potential energy of the model is quadratic with respect to the degrees of freedom, such that the minimization is done after solving a single linear problem.

3. For the nodes in the contact domain in the end of a time step the following logic is used to update their contact status.

- If a node was sticking to the surface of a pulley or had no contact before the time step, then we check the finite element estimation of  $q = -\partial_s Q$  in the node. If  $-f \leq q \leq f$ , the new status is *stick*, otherwise we switch to *slip forward/backward* depending on the sign of  $q$ .
- If a node was slipping, we check its displacement since the previous time step and compare it to the actual displacement of the surface of the pulley  $\tau\omega_{1,2}r$ . If the inequality corresponds to the direction of slipping (forward or backward), the contact state remains in its previous status, otherwise we switch it to *stick*.

This explicit scheme of time integration of the frictional process is simple in comparison to the mathematically advanced schemes based on the Kuhn—Tucker conditions, see e.g. (Pfeiffer and Glocker, 2004; Yastrebov, 2013). Moreover, it appears to be more robust and efficient in comparison to an implicit one, which features iterations within each time step aiming at performing it with such contact states, which are consistent with the new deformed state of the strip. As shown below, one achieves plausible results, which in general correspond to the expected behaviour and solutions, obtained using different schemes.

Considering a belt drive with the total length of the contour  $L = 6$  (the SI system of units is used throughout the paper), the lengths of the contact domains  $\pi r = 1$ , the velocities of the surfaces of the pulleys  $\omega_1 r = 1$ ,  $\omega_2 r = 0.9$ , the tension stiffness of the belt  $b = 1$  and the maximal friction force per unit length  $f = 0.2$ , we solved the problem using  $n = 600$  finite elements and the time step intervals  $\tau = 10^{-3}$ , which provides nearly converged results of the time integration. The computed distributions of the strain along the contour of the belt drive are presented in Fig. 2 for three instances of time: shortly after the pulleys begin rotating, in an intermediate state and after a longer time period, when the system has reached its stationary regime of motion. The evolution of

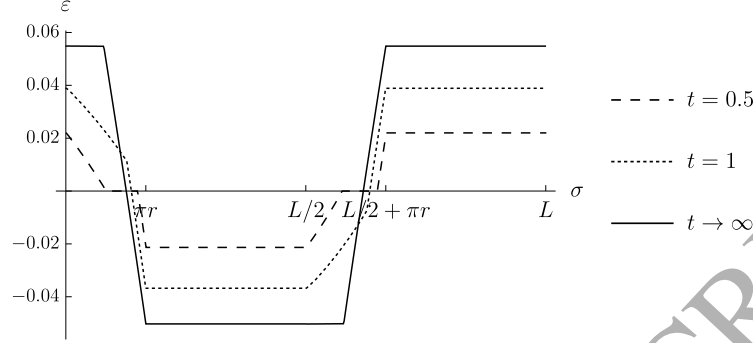


Figure 2: Strain distributions along the contour at three time instances, obtained using a Lagrangian simulation

the deformed state corresponds to the above qualitative analysis. Strains are constant within the free spans, where  $q = 0$ . Three zones, which exist initially in each contact domain, turn into two in the course of the motion, and the stationary strain distribution consists of two constant and two almost linear parts (when the looping of the coordinate  $\sigma$  is accounted for). The difference in the stationary values of strains  $\varepsilon_+(\infty) - \varepsilon_-(\infty) \approx 0.1$  corresponds to the 10% difference in the velocities of the pulleys.

Now we analyze the time evolution of the sizes of the zones of slip  $c$  at both pulleys. Explicit time integration and motion of nodes across the boundary between the slip and stick regions result in an oscillatory signal, which resembles a staircase because of the finite element discretization (see Fig. 10 below for an example of such solutions). The smooth curves in Fig. 3 resulted from low pass filtering of the computed time histories with a suitable time constant. The slight difference between the two pulleys is shown in detail in the zoomed area (the difference vanishes at smaller strains, which are studied in the subsequent sections below; we decided to consider large strains here to demonstrate this nonlinear effect). The small "kinks" in the solution are visible when the middle contact zones with  $\varepsilon = 0$  collapse at a time instant  $t = t^*$ , and the desired stationary values  $c \approx 0.5$  are determined by the choice of the maximal friction force  $f$ : the total friction force is approximately  $(\pi r - c)f \approx 0.1$ , which equals

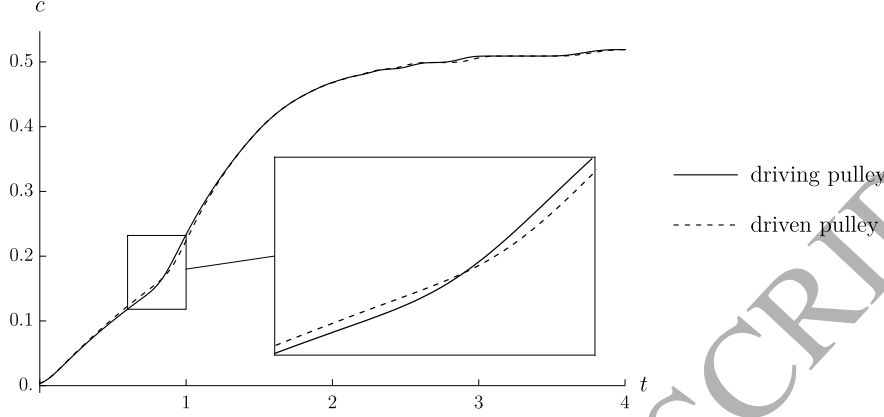


Figure 3: Time evolution of the sizes of the slipping regions at both pulleys

to the tension difference between the free spans  $b\varepsilon_+(\infty) - b\varepsilon_-(\infty)$ .

Next we address the time histories of the strains within the free spans, Fig. 4. The stationary value of  $\varepsilon_+$  exceeds 0.05 because of the geometric nonlinearity and would approach  $(\omega_1/\omega_2 - 1)/2$  when the difference between the velocities of the pulleys is smaller. The seemingly smooth solution contains a high-frequency saw-like component, visible in the zoomed part. The latter appears because of the switching contact conditions as the nodes are entering and leaving the contact regions. Similar numerically induced irregularities may be observed in other solutions, reported in the literature, see e.g. (Dufva et al., 2007; Kubas, 2017). Looking relatively harmless, this effect becomes strongly pronounced in the time derivatives. The velocity of the first node of the finite element mesh

$$v_1 = \frac{d\sigma_1(t)}{dt} \equiv \dot{\sigma}_1 \quad (11)$$

is presented as a function of time in Fig. 5. Obtained using the numerical differentiation of the time series, the signal is highly oscillatory because of the irregular solution. The dashed lines present the upper and lower envelopes of the signal, computed using a suitable time window. The solid line, which results from processing the numerical time derivatives using a low pass filter with a suitable time constant, corresponds to the subsequent analytical results and

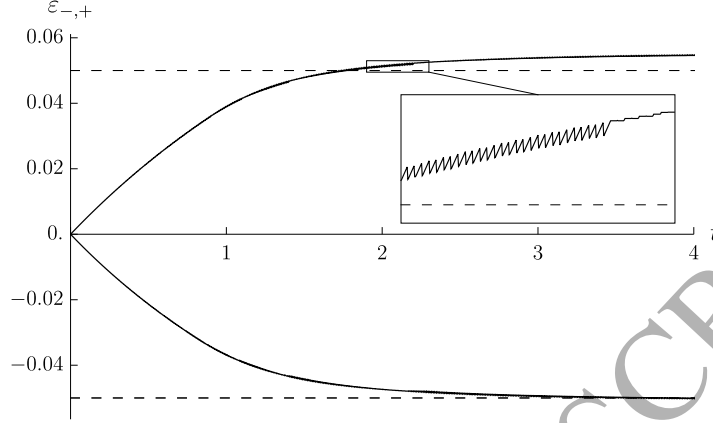


Figure 4: Time history of the strains in the tight and slack spans of the drive

Eulerian finite element computations. In a stationary process, the velocity of the particle remains constant between the free spans and the sticking zones, and the particle accelerates or decelerates in the slipping zones of sliding friction.

Now we clearly see the two essential drawbacks of the Lagrangian approach to the problem at hand:

- the mesh size needs to be kept constant in the entire domain, which is particularly inconvenient when the contact regions become very small in comparison to the free spans;
- numerically induced oscillations become particularly difficult to handle in dynamical problems because of their resonances with the higher part of the spectrum of the finite element model.

While mortar and other methods may help overcoming the latter issue, the use of Eulerian (or more generally mixed Eulerian-Lagrangian) kinematics eradicates the roots for both mentioned obstacles.

#### 4. Analytical study

In this section we use simplifying assumptions given above in Sect. 3 in order to find an analytical (or semi-analytical) solution of the transient problem at

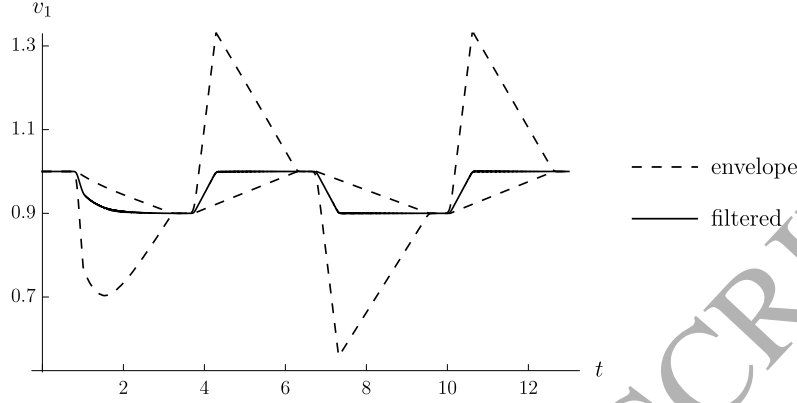


Figure 5: Velocity of the first node  $v_1$ : upper and lower envelopes of the highly oscillatory time series and filtered signal

hand. We consider the relative difference between the angular velocities to be small. The strain of the belt is then small too and we neglect higher-order terms when appropriate.

The analytical models presented below are based on an Eulerian description, at which we follow the mechanical process at a given point of the contour  $\sigma$ . Knowing the current material coordinate of a particle at a given point in space,

$$s = s(\sigma, t), \quad (12)$$

we determine the kinematics of the belt motion. The above relation is an inverse of the material description Eq. (6) at  $t = \text{const}$ . Then  $\partial_s \sigma = (\partial_\sigma s)^{-1}$ , and for the strain we find

$$\partial_\sigma s = \frac{1}{1 + \varepsilon}. \quad (13)$$

We also transform the velocity Eq. (7) to the new description. The time derivative is determined using the chain rule:

$$\begin{aligned} 0 = \partial_t s(\sigma, t) &= \partial_\sigma s \partial_t \sigma + \partial_t s, \quad \partial_t s \equiv \left. \frac{\partial s}{\partial t} \right|_{\sigma=\text{const}} \Rightarrow \\ \Rightarrow v &= -(\partial_\sigma s)^{-1} \partial_t s = -(1 + \varepsilon) \partial_t s. \end{aligned} \quad (14)$$

The local time derivative  $\partial_t$  is considered in a given point in space in opposite to the material one  $\partial_t$ .



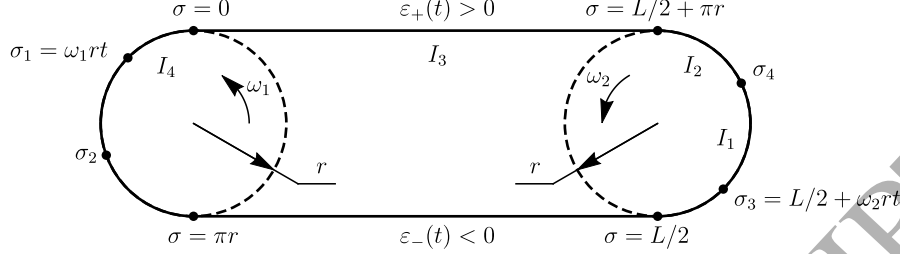


Figure 6: First stage of transient process with pre-historic zones in the contact domains

#### 4.1. Analytical solution for the first stage with zones of vanishing strains

Consider the belt drive shown in Fig. 6. Currently we focus the attention on the initial stage of the simulation. Sticking contact dominates initially in the contact regions. Zones of slip arise and expand on the pulleys as the system is brought into motion. Stick means that the strains of the free spans  $\varepsilon_{+,-}$  are translated with the velocity of the pulley surface in  $(0, \sigma_1)$  and  $(L/2, \sigma_3)$ , and the upper boundaries of both zones grow linearly in time during the first stage of motion; see Eq. (23) below. The uniform friction force is applied on the belt in the slip zones  $(\sigma_2, \pi r)$  and  $(\sigma_4, L/2 + \pi r)$ . In this subsection we consider the motion until the time instant when the zones of initial strain  $(\sigma_1, \sigma_2)$  and  $(\sigma_3, \sigma_4)$  collapse.

We recall the constitutive relation Eq. (4) and the equation of balance of forces Eq. (8) from Sect. 2 and Sect. 3. Developing the analytical solution in the range of small strains, we act as it is common in linearized elasticity and treat the derivatives with respect to the material and spatial coordinates as identical. Replacing thus  $\partial_s$  by  $\partial_\sigma$  in Eq. (8), substituting Eq. (4) and considering  $q = -f$  in the domain  $(\sigma_4, L/2 + \pi r)$ , in which the belt moves faster than the pulley surface, we find the relation between the size of the slipping zone and the strain in the tight span:

$$\begin{aligned} \partial_\sigma(b\varepsilon) &= f, \quad \varepsilon|_{\sigma=\sigma_4} = 0, \quad \varepsilon|_{\sigma=L/2+\pi r} = \varepsilon_+ \Rightarrow \\ \Rightarrow \quad \varepsilon_+ &= \frac{f}{b} \left( \frac{L}{2} + \pi r - \sigma_4 \right) \Rightarrow \quad \sigma_4 = \frac{L}{2} + \pi r - \frac{b}{f} \varepsilon_+. \end{aligned} \quad (15)$$

The foregoing analysis is based on the consideration of the total material length of the half of the belt in the counter-clockwise direction between the points  $\sigma_3$  and  $\sigma_1$ , which is conserved as the material particles at its boundaries are fixed:

$$\sum_{k=1}^4 I_k = \frac{1}{2}L. \quad (16)$$

We introduced a denotation for the material lengths of the enumerated segments (see Fig. 6):

$$I_k = \int_{\sigma_{k-1}}^{\sigma_k} \partial_\sigma s \, d\sigma = \int_{\sigma_{k-1}}^{\sigma_k} (1 - \varepsilon) \, d\sigma, \quad (17)$$

the linearized counterpart of Eq. (13) accounting for the smallness of strains has been used. We differentiate Eq. (16) with respect to time,

$$\sum_{k=1}^4 \dot{I}_k = 0, \quad (18)$$

and consider all four segments individually. Following Eq. (11), we use a dot for the time derivatives of variables, which depend only on time.

In the first segment we have zero pre-historic strain, therefore

$$I_1 = \sigma_4 - \sigma_3, \quad \dot{I}_1 = -\frac{b}{f}\dot{\varepsilon}_+ - \omega_2 r. \quad (19)$$

For the second segment we write the integral Eq. (17) as

$$I_2 = \int_{\sigma_4}^{L/2+\pi r} \left(1 - \frac{f}{b}(\sigma - \sigma_4)\right) d\sigma, \quad (20)$$

and its time derivative reads

$$\dot{I}_2 = -\dot{\sigma}_4 + \frac{f}{b}\dot{\sigma}_4 \left(\frac{L}{2} + \pi r - \sigma_4\right) = \frac{b}{f}(1 - \varepsilon_+)\dot{\varepsilon}_+. \quad (21)$$

The third segment is the tight span with the constant strain  $\varepsilon_+$ , and

$$\begin{aligned} I_3 &= \left(\frac{L}{2} - \pi r\right)(1 - \varepsilon_+), \\ \dot{I}_3 &= -\left(\frac{L}{2} - \pi r\right)\dot{\varepsilon}_+. \end{aligned} \quad (22)$$

The derivation for the fourth segment is challenging at most. In  $0 \leq \sigma \leq \sigma_1 = \omega_1 r t$  the belt is transported by the surface of the pulley, and the strain here is the strain in the tight span with a certain time delay:

$$\varepsilon(\sigma, t) = \varepsilon_+ \left( t - \frac{\sigma}{\omega_1 r} \right); \quad (23)$$

$\varepsilon_+(t)$  is a function of time. Now we compute

$$I_4 = \int_0^{\omega_1 r t} \left( 1 - \varepsilon_+ \left( t - \frac{\sigma}{\omega_1 r} \right) \right) d\sigma. \quad (24)$$

Both the integrand and the upper limit of integration depend on time, which needs to be accounted for when computing the time derivative:

$$\dot{I}_4 = \omega_1 r (1 - \varepsilon_+(0)) - \int_0^{\omega_1 r t} \dot{\varepsilon}_+ \left( t - \frac{\sigma}{\omega_1 r} \right) d\sigma. \quad (25)$$

Further we use the identity

$$\partial_\sigma \varepsilon_+ \left( t - \frac{\sigma}{\omega_1 r} \right) = -\frac{1}{\omega_1 r} \dot{\varepsilon}_+ \left( t - \frac{\sigma}{\omega_1 r} \right) \quad (26)$$

to transform the time derivative under the integral in Eq. (24) to a spatial one. This allows to compute the integral, and we arrive at a simple expression

$$\dot{I}_4 = \omega_1 r (1 - \varepsilon_+(t)). \quad (27)$$

Finally we add Eqs. (19), (21), (22) and (27) together and obtain an initial value problem for the strain at the tight span:

$$\begin{aligned} \left( \frac{L}{2} - \pi r \right) \dot{\varepsilon}_+ + \frac{b}{f} \varepsilon_+ \dot{\varepsilon}_+ + \omega_1 r \varepsilon_+ &= \omega_1 r - \omega_2 r; \\ \varepsilon_+(0) &= 0. \end{aligned} \quad (28)$$

This is the Abel equation of the second kind, whose exact solution can be written in terms of the Lambert-W function (also known as product logarithm). We do not present this solution here for the sake of brevity.

The strain has the order of smallness of the relative difference between the angular velocities of the pulleys. Neglecting in Eq. (28) the nonlinear term with

$\varepsilon_+ \dot{\varepsilon}_+$  and solving the linear problem, we find a simple closed-form solution

$$\varepsilon_+ = \frac{\omega_1 - \omega_2}{\omega_1} \left( 1 - \exp \left( \frac{2\omega_1 r t}{2\pi r - L} \right) \right). \quad (29)$$

Let us have a closer look at the nonlinear term  $b f^{-1} \varepsilon_+ \dot{\varepsilon}_+$  in Eq. (28). As mentioned previously, we are focusing the analysis on the case, when significant part of the contact region is sliding. The friction force  $f$  times  $r$  is then of the order of magnitude of the tension force  $b \varepsilon_+$ , which means that the nonlinear term shall not be neglected in this case. Nevertheless, the linear solution Eq. (29) is expected to be valid at larger  $f$ . It shall also be accurate in the beginning of a simulation, when  $\varepsilon_+$  is small. Summarizing both, we say that the linear solution is accurate as long as the sliding zone is small, which is justified by the comparison with other simulation results below in Fig. 9.

If we consider the rest part of the belt  $\sigma_1 \leq \sigma \leq \sigma_3$  in the same way, we end up with an equation for  $\varepsilon_-(t)$ , which is similar to Eq. (28). The closed-form solution of its linearized form reads

$$\varepsilon_- = \frac{\omega_2 - \omega_1}{\omega_2} \left( 1 - \exp \left( \frac{2\omega_2 r t}{2\pi r - L} \right) \right). \quad (30)$$

The time instance  $t^*$ , at which the points  $\sigma_3$  and  $\sigma_4$  meet, is determined by

$$\pi r - \frac{b}{f} \varepsilon_+(t^*) = \omega_2 r t^*; \quad (31)$$

the equation Eq. (28) is valid until this time instance. For the time instance  $t^{**}$ , at which the points  $\sigma_1$  and  $\sigma_2$  coincide and the pre-historic zone vanishes at the driving pulley, we write

$$\pi r + \frac{b}{f} \varepsilon_-(t^{**}) = \omega_1 r t^{**}. \quad (32)$$

If we substitute the linearized solutions Eq. (29) and Eq. (30) into the equations Eq. (31) and Eq. (32) respectively, then we see: these time instances are close to each other in the case of close pulley velocities, and the relative difference between  $t^*$  and  $t^{**}$  is of the same order as the relative difference between  $\omega_1$  and  $\omega_2$ .

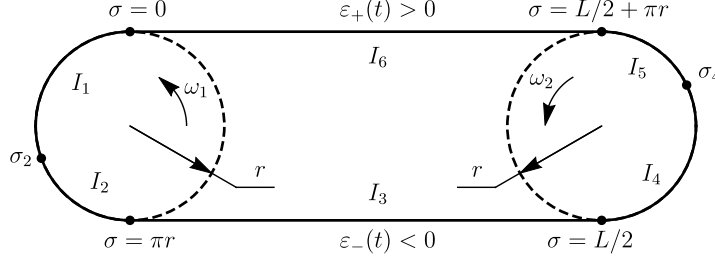


Figure 7: Second stage of transient process with no pre-historic zones of vanishing strains

The conclusion was confirmed in a series of numerical experiments. Integrating Eq. (28) and its counterpart in the second belt part over time and using conditions Eq. (31) and Eq. (32), we computed  $t^*$  and  $t^{**}$  for various combinations of parameters. Significant difference between the two time instances appears only in the case of an extremely compliant belt.

#### 4.2. Analytical solution for the second stage of the transient process

The short period of time between the instances  $t^*$  and  $t^{**}$ , during which the pre-historic zone with vanishing strains exists just on a single pulley, is at first left out of consideration. We proceed to the state when the segments of initial deformation  $(\sigma_1, \sigma_2)$  and  $(\sigma_3, \sigma_4)$  with  $\varepsilon = 0$  have already collapsed, see Fig. 7. The boundaries between the zones of stick and slip in the contact region are now denoted by  $\sigma_2$  and  $\sigma_4$ .

Similar to Eq. (15), we use the continuity of strain at the points  $\sigma_2$ ,  $\pi r$ ,  $\sigma_4$ , and  $L/2 + \pi r$  and write

$$\begin{aligned}\varepsilon_- &= \varepsilon(\sigma_2, t) - \frac{f}{b}(\pi r - \sigma_2), \\ \varepsilon_+ &= \varepsilon(\sigma_4, t) + \frac{f}{b}\left(\frac{L}{2} + \pi r - \sigma_4\right),\end{aligned}\tag{33}$$

in which we have

$$\begin{aligned}\varepsilon(\sigma_2, t) &= \varepsilon_+ \left(t - \frac{\sigma_2}{\omega_1 r}\right), \\ \varepsilon(\sigma_4, t) &= \varepsilon_- \left(t - \frac{\sigma_4 - L/2}{\omega_2 r}\right).\end{aligned}\tag{34}$$

The relations Eq. (34) implicitly relate  $\sigma_2$  and  $\sigma_4$  to  $\varepsilon_+$  and  $\varepsilon_-$  (or vice versa).

Let us differentiate Eq. (33) with respect to time:

$$\begin{aligned}\dot{\varepsilon}(\sigma_2, t) &= \dot{\varepsilon}_- - \frac{f}{b} \dot{\sigma}_2, \\ \dot{\varepsilon}(\sigma_4, t) &= \dot{\varepsilon}_+ + \frac{f}{b} \dot{\sigma}_4.\end{aligned}\tag{35}$$

We derive the differential equation considering the constant material length of the entire belt. Using the definition of material lengths of individual segments  $I_k$  from Eq. (17), we write

$$\dot{L} = \sum_{k=1}^6 \dot{I}_k = 0.\tag{36}$$

The segments are treated in the same manner as when deriving Eq. (28). In the first segment  $(0, \sigma_2)$  (stick zone on the driving pulley) we again have the translation of the strain with the pulley motion and, analogously to Eq. (27), we find

$$\dot{I}_1 = \dot{\sigma}_2 (1 - \varepsilon(\sigma_2, t)) + \omega_1 r (\varepsilon(\sigma_2, t) - \varepsilon_+).\tag{37}$$

The constant load appears in the second segment (slip zone):

$$\dot{I}_2 = -\dot{\sigma}_2 (1 - \varepsilon(\sigma_2, t)) - (\pi r - \sigma_2) \left( \frac{f}{b} \dot{\sigma}_2 + \dot{\varepsilon}(\sigma_2, t) \right).\tag{38}$$

The third segment is the slack span with the constant strain  $\varepsilon_-$ , therefore

$$\dot{I}_3 = \left( \pi r - \frac{L}{2} \right) \dot{\varepsilon}_-.\tag{39}$$

We do the similar transformations for the second half of the belt and obtain the differential equation

$$\begin{aligned}0 = \dot{L} &= \sum_{k=1}^6 \dot{I}_k = \omega_1 r (\varepsilon(\sigma_2, t) - \varepsilon_+) + \omega_2 r (\varepsilon(\sigma_4, t) - \varepsilon_-) + \\ &+ \left( \sigma_2 - \frac{L}{2} \right) \dot{\varepsilon}_- + (\sigma_4 - L) \dot{\varepsilon}_+.\end{aligned}\tag{40}$$

Both unknown strains  $\varepsilon_+$  and  $\varepsilon_-$  are to be treated together in the present analysis, and another relation is needed to close the system of equations. We proceed with the following statement:

$$s \Big|_{\sigma=L/2} - s \Big|_{\sigma=0} = \int_0^{L/2} \partial_\sigma s \, d\sigma = \sum_{k=1}^3 I_k.\tag{41}$$

Then we differentiate this equation with respect to time accounting for the first line of Eq. (14):

$$-(\partial_\sigma s \partial_t \sigma) \Big|_{\sigma=L/2} + (\partial_\sigma s \partial_t \sigma) \Big|_{\sigma=0} = \sum_{k=1}^3 \dot{I}_k. \quad (42)$$

Since we know the velocities  $v = \omega_{1,2}r$  in the stick zones at the points  $\sigma = 0$  and  $\sigma = L/2$ , using the second line of Eq. (14) we write

$$\omega_1 r(1 - \varepsilon_+) - \omega_2 r(1 - \varepsilon_-) = \sum_{k=1}^3 \dot{I}_k. \quad (43)$$

Substituting the computed above  $\dot{I}_k$  in Eqs. (37), (38) and (39) into Eq. (43), we arrive at the equality

$$\omega_1 r(1 - \varepsilon(\sigma_2, t)) - \omega_2 r(1 - \varepsilon_-) + \left(\frac{L}{2} - \sigma_2\right) \dot{\varepsilon}_- = 0. \quad (44)$$

By adding Eq. (40) to Eq. (44) we finally obtain

$$\omega_1 r(1 - \varepsilon_+) - \omega_2 r(1 - \varepsilon(\sigma_4, t)) + (\sigma_4 - L) \dot{\varepsilon}_+ = 0. \quad (45)$$

We rewrite the derived system Eqs. (44), (45) in the normal form:

$$\begin{aligned} \dot{\varepsilon}_- &= \frac{-\omega_1 r(1 - \varepsilon(\sigma_2, t)) + \omega_2 r(1 - \varepsilon_-)}{L/2 - \sigma_2}, \\ \dot{\varepsilon}_+ &= \frac{\omega_1 r(1 - \varepsilon_+) - \omega_2 r(1 - \varepsilon(\sigma_4, t))}{L - \sigma_4}. \end{aligned} \quad (46)$$

For the time-dependent functions  $\varepsilon_-$ ,  $\varepsilon_+$ ,  $\sigma_2$ ,  $\sigma_4$  we have two differential equations Eq. (46) together with two algebraic equations Eq. (33) and a denotation Eq. (34).

It is important that the proposed solution scheme may be applied for the entire simulation beginning from  $t = 0$ . The results for the first stage follow as we simply set both  $\varepsilon_{+,-}$  equal to zero as long as the argument of the function is negative in Eq. (34), which automatically results in the zones with vanishing pre-historic strains. The equivalence of both solutions during the first stage  $t \leq \min(t^*, t^{**})$  is indeed justified by the simulation results in Fig. 9. Moreover, the initial time derivatives of the strain for both Eq. (46) and Eq. (28) are identical:

$$\dot{\varepsilon}_+(0) = -\dot{\varepsilon}_-(0) = \frac{\omega_1 r - \omega_2 r}{L/2 - \pi r}. \quad (47)$$

#### 4.3. Numerical scheme

We solve the system of equations Eqs. (33), (34) and (46) numerically using the explicit midpoint time integration scheme. The below algorithm has been implemented in the framework of the computer algebra environment *Wolfram Mathematica*<sup>1</sup>.

The first intermediate half-step step begins as follows:

$$\begin{aligned}\varepsilon_{-, \tau/2} &= \frac{\tau - \omega_1 r + \omega_2 r}{2} \frac{L/2 - \pi r}{L/2 - \pi r}, \\ \varepsilon_{+, \tau/2} &= \frac{\tau \omega_1 r - \omega_2 r}{2} \frac{L/2 - \pi r}{L/2 - \pi r}.\end{aligned}\quad (48)$$

Here  $\tau$  is the size of the time step of the numerical method. We collect each newly obtained value at a half or a full step to a set of data, which is then linearly interpolated to provide the history of the values  $\varepsilon_{+,-}$ . The interpolated functions are then used for solving the system of equations Eq. (33), Eq. (34) with the Newton method by means of the built-in function *FindRoot*. Clearly, non-trivial values from the data set will be retrieved only during the second stage of the solution, and the data is just accumulated during the first stage  $t < \min(t^*, t^{**})$ . The numerical solver provides now the half-step values  $\sigma_2$  and  $\sigma_4$  at  $t = \tau/2$ , and the strains after the first full step are

$$\begin{aligned}\varepsilon_{-, \tau} &= \tau \frac{-\omega_1 r \left(1 - \varepsilon_+ \left(\frac{\tau}{2} - \frac{\sigma_{2, \tau/2}}{\omega_1 r}\right)\right) + \omega_2 r (1 - \varepsilon_{-, \tau/2})}{L/2 - \sigma_{2, \tau/2}}, \\ \varepsilon_{+, \tau} &= \tau \frac{\omega_1 r (1 - \varepsilon_{+, \tau/2}) - \omega_2 r \left(1 - \varepsilon_- \left(\frac{\tau}{2} - \frac{\sigma_{4, \tau/2} - L/2}{\omega_2 r}\right)\right)}{L - \sigma_{4, \tau/2}}.\end{aligned}\quad (49)$$

Now we interpolate the time histories of the strains again and determine the coordinates of the boundary points  $\sigma_{2, \tau}$  and  $\sigma_{4, \tau}$  by the Newton method.

Repeating the computations, we obtain the values  $\varepsilon_{+,-}$  at each time step of the simulation. The results of the numerical study are presented in Fig. 9 in comparison with other methods proposed in this paper.

<sup>1</sup><https://www.wolfram.com/mathematica>



## 5. Eulerian finite element model

In the following we use the sample problem at hand and develop a strategy to model dry friction in the framework of a non-material finite element formulation and validate the results against above analytical solutions. In the future work, the strategy will be used within a general mixed Eulerian-Lagrangian formulation (Vetyukov et al., 2016, 2017a), see the final parts of the Introduction above and Conclusions below for a discussion.

At spatial description Eq. (12) we discretize the contour  $0 \leq \sigma \leq L$  into unequal finite elements with a linear approximation for  $s(\sigma)$ . The free spans have constant strains, the mapping  $s(\sigma)$  is exactly linear there and we need just a single finite element for each free span. The contact regions are separately discretized into  $n$  finite elements each with nodal positions  $\sigma_{k,\alpha}$ ;  $k = 0 \dots n$  is the index of a node on a pulley  $\alpha = 1, 2$ . The first and the last nodes lie at the boundaries of the contact regions:

$$\sigma_{0,1} = 0, \quad \sigma_{n,1} = \pi r, \quad \sigma_{0,2} = L/2, \quad \sigma_{n,2} = L/2 + \pi r, \quad (50)$$

see Fig. 1.

The looping conditions need to be taken into account. The points of the contour  $\sigma$  and  $\sigma + L$  are identical, as well as the material points  $s$  and  $s + L$ . We facilitate the use of a looped mesh and avoid the complexity intrinsic to the above Lagrangian presentation Eq. (10) by introducing a new variable,

$$s = \sigma + \bar{s}(\sigma, t). \quad (51)$$

Now we consider  $\bar{s}$  as the primary unknown field, which needs to be periodic:  $\bar{s}(\sigma, t) = \bar{s}(\sigma + L, t)$ , and

$$\partial_\sigma s = \partial_\sigma \bar{s} + 1, \quad \varepsilon = (1 + \partial_\sigma \bar{s})^{-1} - 1, \quad \bar{s}|_{t=0} = 0. \quad (52)$$

The finite element model contains  $2n + 2$  nodal unknowns  $\bar{s}_{k,\alpha}$ . The strain at a pulley  $\alpha$  on an element  $e = 1 \dots n$  reads

$$\begin{aligned} \varepsilon_{e,\alpha} &= (1 + (\partial_\sigma \bar{s})_{e,\alpha})^{-1} - 1, \\ (\partial_\sigma \bar{s})_{e,\alpha} &= (\bar{s}_{e,\alpha} - \bar{s}_{e-1,\alpha})/h, \quad h = \pi r/n, \end{aligned} \quad (53)$$

and the strains at the free spans are

$$\begin{aligned}\varepsilon_{+,-} &= (1 + (\partial_\sigma \bar{s})_{+,-})^{-1} - 1, \\ (\partial_\sigma \bar{s})_+ &= (\bar{s}_{0,1} - \bar{s}_{n,2})/(L/2 - \pi r), \quad (\partial_\sigma \bar{s})_- = (\bar{s}_{0,2} - \bar{s}_{n,1})/(L/2 - \pi r).\end{aligned}\tag{54}$$

The total strain energy of the belt

$$U^{\text{strain}} = \int_0^L \frac{1}{2} b \varepsilon^2 \partial_\sigma s \, d\sigma \tag{55}$$

is easy to integrate as the strains are constant in each finite element:

$$\begin{aligned}U^{\text{strain}} &= \frac{1}{2} b \sum_{e=1}^n h \varepsilon_{e,\alpha}^2 (1 + (\partial_\sigma \bar{s})_{e,\alpha}) + \\ &+ \frac{1}{2} b (\varepsilon_+^2 (1 + (\partial_\sigma \bar{s})_+) + \varepsilon_-^2 (1 + (\partial_\sigma \bar{s})_-)) (L/2 - \pi r)\end{aligned}\tag{56}$$

The clear advantage of the Eulerian modelling is that all finite elements but the two special ones (free spans) always remain in contact with the pulleys. The contact domains are separated into zones of sticking  $\Omega^{\text{stick}}$  and sliding forward and backward  $\Omega^{\text{slip}}$ . Similar to Eq. (9), at each time step we minimize the total strain energy plus the potential of sliding friction forces accounting for the kinematic conditions in  $\Omega^{\text{stick}}$ . An iterative Newton minimization scheme needs to be used this time, as  $U^{\text{strain}}$  is no longer a quadratic function of degrees of freedom. This, however, cannot speak for the advantage of the Lagrangian model as it would also require Newton minimization as soon as more complicated forms of deformation of the belt are considered. Aiming at more sophisticated finite element schemes, which feature not only displacements as nodal degrees of freedom, we impose the kinematic conditions in the integration points of the finite elements in the form of a penalty-like contribution to the total energy of the system. At each time step we minimize a function of all nodal unknowns

$$\begin{aligned}U(\bar{s}_{k,\alpha}) &= U^{\text{strain}} + U^{\text{contact}} \rightarrow \min, \\ U^{\text{contact}} &= \int_{\Omega^{\text{stick}}} P^{\text{stick}} \, d\sigma + \int_{\Omega^{\text{slip}}} P^{\text{slip}} \, d\sigma.\end{aligned}\tag{57}$$

Both contact potentials are formulated in terms of the displacement  $u$  of a particle of the belt at a given position  $\sigma$  within a time step. Its smallness

allows linearizing the kinematic relation for  $u$ . The computation begins with the velocity of a particle Eq. (14) with the transformation Eq. (51) to a new variable:

$$v = -(1 + \partial_\sigma \bar{s})^{-1} \partial_t \bar{s}. \quad (58)$$

Denoting by the superscript "0" the values in the beginning of a time step, we find the linearized displacement of a material point within a time step:

$$u = \tau v^0 = -(1 + (\partial_\sigma \bar{s})^0)^{-1} (\bar{s} - \bar{s}^0). \quad (59)$$

Now the displacement is determined by the primary unknown field  $\bar{s}$  and by its known values in the beginning of a time step, both being interpolated from the nodal values  $\bar{s}_{k,\alpha}$  and  $\bar{s}_{k,\alpha}^0$ . The penalty potential, which makes the belt moving together with the surface of the pulleys, reads

$$P^{\text{stick}} = \frac{1}{2} K (u^{\text{rel}})^2, \quad u^{\text{rel}} \equiv u - \tau \omega_{1,2} r. \quad (60)$$

Here  $K$  is a large penalty factor, which can be considered as the high stiffness of a regularizing elastic layer between the belt and the pulleys, and  $u^{\text{rel}}$  is a displacement relative to the surface of the pulleys.

The potential of the sliding friction forces is linear in the displacement:

$$P^{\text{slip}} = \pm f u, \quad (61)$$

the sign is chosen depending on whether the belt slips forward or backward. Integrating  $P^{\text{slip}}$  over  $\sigma$  in Eq. (57), we count the sliding friction force per unit length of the contour of the pulley. This is thus not in line with the above Lagrangian model, in which the friction forces act per unit material length of the belt. Avoiding the discussion, which of the two options is more consistent from the tribological point of view, we simply point out that the present Eulerian formulation can easily be adopted to the above option by introducing a factor  $\partial_\sigma s$  in Eq. (61) and below in switching conditions, and that the choice does not lead to noticeable changes in the simulation results at realistically small values of the strain of the belt.

The integrals in Eq. (57) are computed using the Gaussian quadrature rule, just a single integration point in the middle of each element is used for the present linear finite element approximation. In general, we need to evaluate  $u$  as well as its derivatives, required for the numerical minimization, in the integration points.

Having solved the static problem Eq. (57), we obtain the new state of static equilibrium of the belt in the end of a time step. In line with the explicit scheme of time integration, we must conclude on the new contact state in each integration point of the model. The decision is made similar to the conditions in Sect. 3.

- If the integration point was *sticking*, we check whether the new value of the contact force  $q = Ku^{\text{rel}}$  is not exceeding the limits. As long as  $-f \leq q \leq f$ , the integration point remains in the sticking state, otherwise we switch to *slip forward* or *slip backward*.
- If the node was *slipping*, we check whether the sign of the actually reached displacement relative to the pulley surface  $u^{\text{rel}}$  corresponds to the previous direction of slipping, and decide whether *slipping* in the same direction continues or else we switch to *stick*.

Robustness and accuracy of the exposed relatively simple numerical scheme with the explicit time integration depend on the interplay of the numerical parameters, namely the time step size  $\tau$ , the finite element grid size  $h$  and the penalty stiffness  $K$ . Smaller values of  $K$  result in more stable time integration, but the additional flexibility in the contact domain smoothens the solution (see discussion of Fig. 8 below) and also leads to the effect of numerical drift: the non-vanishing value of  $u^{\text{rel}}$  in the end of a time step in the sticking zone is an inaccuracy of the solution, which is accumulated during the time integration as the preceding values  $\bar{s}^0$  were already inaccurate. This can be avoided by keeping track of the previously accumulated  $u^{\text{rel},0}$ , taking it into account in Eq. (60), updating it in each time step and advecting (transporting) the field numerically during the time integration. While being more accurate, the modified version of

the algorithm becomes significantly more complicated for the implementation. In the simulations below we achieve accurate solutions by using sufficiently high penalty stiffness factor  $K$ .

Last but not least, in the numerical experiments we observed that replacing the initial value of the derivative  $(\partial_\sigma \bar{s})^0$  by its actual value  $\partial_\sigma \bar{s}$  in the formulation of a displacement  $u$  in Eq. (59) results in more accurate time integration and allows for larger time steps. This modification of the algorithm towards a partially implicit numerical scheme is simple in a computer algebra environment. The presented below numerical results were, however, obtained with the purely explicit expression Eq. (59) as the time step size was sufficiently small.

## 6. Eulerian finite element simulations with constant speeds of the pulleys

The developed algorithm is sufficiently simple to be implemented using the *Wolfram Mathematica*. The simulation environment allows computing the time evolution of the deformation of the belt and of the contact zones for given parameters and geometry of the model, speeds of the pulleys and parameters of the numerical scheme:  $n, \tau, K$ . Opting for the set of parameters as in Sect. 3, we decided to leave the effect of geometric nonlinearity out of scope for the sake of meaningful comparison of solutions. Therefore we reduced the relative difference in the velocities of the pulley surfaces:

$$\begin{aligned} L = 6, \quad \pi r = 1, \quad b = 1, \quad \omega_1 r = 1, \quad \omega_2 r = 0.999, \\ f = 0.002, \quad n = 50, \quad \tau = 10^{-3}. \end{aligned} \tag{62}$$

The maximal friction force is again chosen such, that the size of the zones of slip would approach the stationary value  $c = 0.5$ . The relation between the length of the belt  $L$  and the radius of the pulleys  $r$  is chosen such that one can easier observe the effects of interest: the collapse of the pre-historic zone of initial strains and the transition to the stationary motion happen soon one after another, which simplifies presenting the results in a single plot. We computed

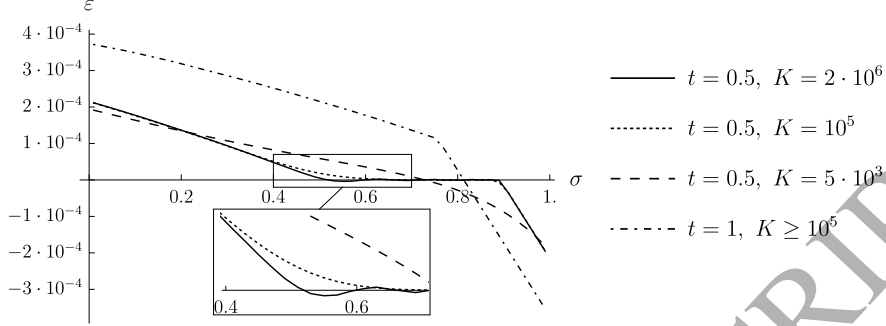


Figure 8: Strain distributions in the first contact region at two instances of time, obtained using an Eulerian simulation with varying penalty stiffness factor; results for two higher values of  $K$  are nearly indistinguishable at  $t = 1$ , when the pre-historic zone of vanishing strain has already collapsed

with three values of the penalty stiffness factor  $K = 10^5/20$ ,  $K = 10^5$  and  $K = 20 \cdot 10^5$  to conclude on the convergence of the solution with respect to it.

In Fig. 8 we expose the resulting distribution of the strain in the region of contact with the driving pulley at two instances of time for both values of  $K$ . Solutions with higher values of  $K$  become nearly identical as the time grows and the pre-historic zones of the vanishing strain collapse. The effect of the penalty stiffness is visible during the first stage of the motion, when there should be no strains in the pre-historic part of the zone of stick: numerically induced elasticity between the belt and the surface of the pulleys blurs the kink in the distribution of  $\varepsilon$ , and we approach the exact solution with growing  $K$  and  $n$ .

All the solution techniques are compared in Fig. 9, see the graphical abstract of the manuscript online for a colored version of the figure, in which the single curves are easier to identify. The time history of the strain in the tight span  $\varepsilon_+(t)$  is computed using the Lagrangian finite element simulation as in Sect. 3, the Eulerian finite element model with two values of  $K$ , the closed-form analytical formula Eq. (29), the ordinary differential equation Eq. (28) and the delay differential equation Eq. (46). The grey vertical line has been plotted at the time instant  $t = t^* \approx 0.831$ , which follows from Eq. (31). Both differen-

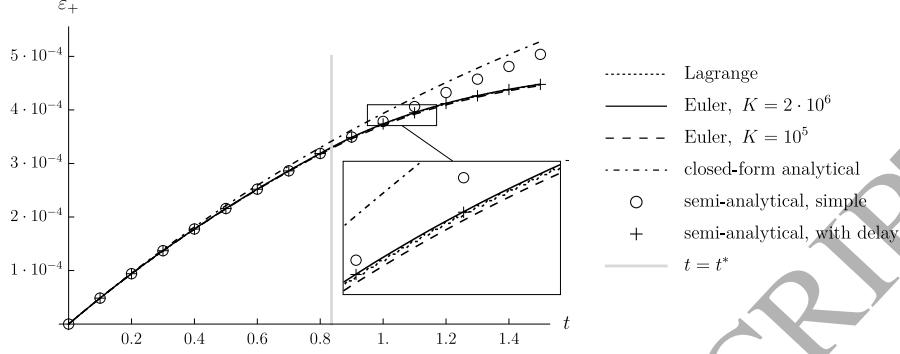


Figure 9: Time history of the strain in the tight span: comparison of Lagrangian finite element solution (*short dashed line*), Eulerian finite element solution with two different values of the penalty stiffness  $K$  (*solid and long dashed lines*), closed-form analytical solution Eq. (29) (*dash-dotted line*) as well as the semi-analytical results of integration of the simple differential equation Eq. (28) (*circles*) and of the delay differential equation Eq. (46) (*crosses*)

tial equations Eq. (28) and Eq. (46) were numerically solved using the explicit midpoint integration with the time step size 0.1. Running the risk of depriving the reader of the pleasure to investigate the results on the own, we nevertheless decided to formulate some remarks.

- The Lagrangian and Eulerian solutions are indeed close to each other, the advantage of the latter one being its smoothness and less finite elements.
- Both Fig. 8 and Fig. 9 convince that the chosen penalty stiffness  $K$  is high enough to classify the solution as nearly converged.
- The closed-form analytical solution Eq. (29) remains accurate as long as the zone of sliding friction is small.
- Results of solving both differential equations Eq. (28) and Eq. (46) are indeed identical and with high degree of accuracy equal to the result of the finite element simulation during the first stage of motion of the system when  $t \leq t^*$ .
- The more complicated delay differential equation needs to be solved dur-

ing the second stage  $t > t^*$ , when the pre-historic part of the contact region with  $\varepsilon = 0$  has collapsed. The results of the Eulerian finite element simulation are almost indistinguishable from the semi-analytical results.

## 7. Harmonically varying speed of driving pulley

In the last numerical example we demonstrate the ability of the model to predict the transient response of the slip zones at the harmonically varying speed  $\omega_1(t)$  of the driving pulley. The speed of the driven pulley is considered constant,  $\omega_2 = 1$ . If not stated otherwise, the same parameter set is applied as in Sect. 6. All results are computed using the Eulerian model, presented in Sect. 5 with  $K = 10^5$ ,  $n = 50$ . The difference between  $\omega_1(t)$  and  $\omega_2$  is small, and the time variation of the size of the slip zones  $c$  is almost identical for both pulleys, but the directions of the slip are opposite. Therefore, in Fig. 10 we show just one single time history per simulation. Because computed  $c$  is a multiple of the element length  $h$ , its time history is plotted as a step function (in contrast to the smoothed presentation of Fig. 3). The area colouring in the plots corresponds to different slip directions along the contact between the belt and the pulley.

Two different cases for the harmonic input of  $\omega_1(t)$  are studied, with two values of the frequency  $\lambda = 1, 2$  each, thus constituting four different simulations. Each time we consider the initial configuration with no slip on the pulleys and a difference  $\omega_1(0) - \omega_2 = 0.001$ . In the first case  $\omega_1(t) = 1.0005 + 0.0005 \cos(\lambda t)$ , i.e. it oscillates between  $\omega_2 = 1$  and 1.001, the results are shown in the first row of Fig. 10. During the simulation, the sign of the relative slip velocity does not change, due to  $\omega_1(t) \geq \omega_2$ . The size of the slip zones  $c$  oscillates around the stationary solution at  $\omega_1 = 1.0005$ , which is the mean value of the harmonic input. The amplitude depends on the frequency  $\lambda$ : it is higher at  $\lambda = 1$ , as the slip zones have more time to develop on the pulleys compared to the simulation with  $\lambda = 2$ .

In the second case  $\omega_1(t) = 1 + 0.001 \cos(\lambda t)$ , i.e. it oscillates around 1 and has



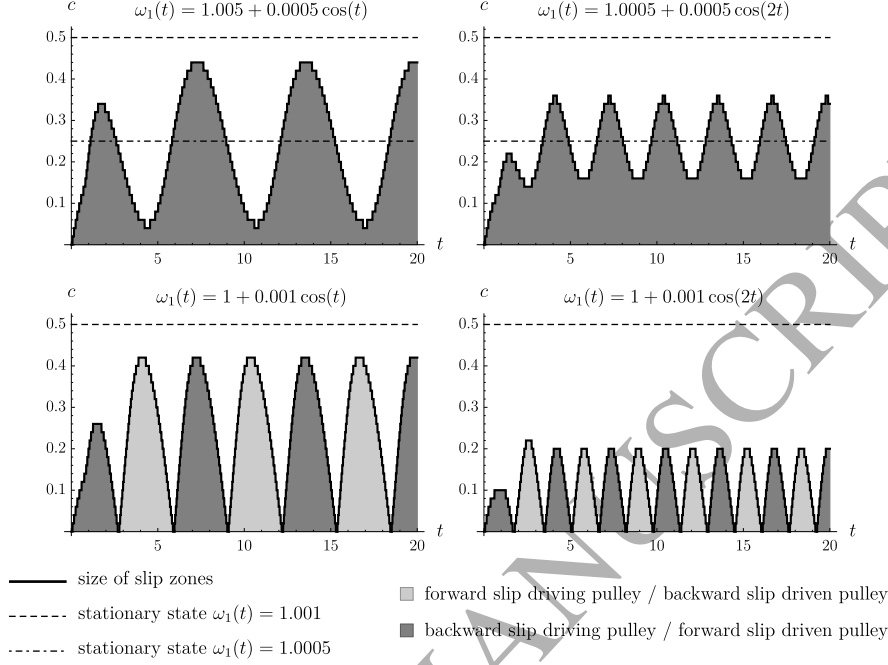


Figure 10: Time history of the slip zone size for time varying  $\omega_1(t)$ . The slip directions are represented by different colours: light grey means forward slip on the driving pulley and backward slip on the driven pulley, dark grey means opposite slip directions.

a maximum value of 1.001, the results are shown in the second row of Fig. 10. The direction of the slip velocity changes, but the time instances of switching are shifted relative to the time points when  $\omega_1(t) = \omega_2$ . Again the size of the slip zones depends on the frequency  $\lambda$ . Similar to the first case, the amplitude of the response gets higher at lower frequency.

## 8. Conclusion

The phenomenon of dry friction plays often an essential role in systems featuring axially moving structures. However, little attention has previously been paid in the literature to the consistency of its treatment in non-material finite element formulations, which are increasingly used in numerical modelling for this kind of problems. On a relatively simple example of an idealized model of

a flexible belt drive, we demonstrate the weakness of the traditional Lagrangian approach. Further we present a novel Eulerian finite element procedure for modelling the quasistatic motion of the belt with time varying zones of stick and slip contact with the pulleys. The obtained smooth solutions were successfully compared against the results of semi-analytical treatment of the problem. The latter analysis is based on the time integration of a nonlinear system of delay differential equations, which were derived in the framework of the present study and shall also be regarded as a novel scientific result.

The investigation is important for more sophisticated modelling scenarios, possibly including the effects of transverse deflection of the belt in the field of gravity, its bending and shear stiffness, out-of-plane deformations and dynamic effects. Combining the present research direction with the semi-analytical solutions of nonlinear contact problems demonstrated by Belyaev et al. (2017), these practically relevant studies will feature the dry friction model as one of the building blocks, which shall be consistent, robust and result in no systematic error of the entire simulations.

### Acknowledgement

The research is carried out in the framework of the joint project of the Russian Foundation for Basic Research (Grant No. 14-51-15001) and the Austrian Science Fund (Grant No. I 2093 International Project).

### References

- Bechtel, S., Vohra, S., Jacob, K., Carlson, C., 2000. The stretching and slipping of belts and fibers on pulleys. *ASME Journal of Applied Mechanics* 67, 197–206.
- Belyaev, A., Eliseev, V., Irschik, H., Oborin, E., 2017. Contact of two equal rigid pulleys with a belt modelled as Cosserat nonlinear elastic rod. *Acta Mechanica* 228, 4425–4434.

- Denoël, V., Detournay, E., 2011. Eulerian formulation of constrained elastica. *International Journal of Solids and Structures* 48, 625–636.
- Dufva, K., Kerkkänen, K., Maqueda, L., Shabana, A., 2007. Nonlinear dynamics of three-dimensional belt drives using the finite-element method. *Nonlinear Dynamics* 48, 449–466.
- Eliseev, V., 2009. A model of elastic string for transmissions with flexible coupling (in Russian). *Scientific and Technical Bulletin of St. Petersburg State Polytechnical University* 84, 192–195.
- Eliseev, V., Vetyukov, Y., 2012. Effects of deformation in the dynamics of belt drive. *Acta Mechanica* 223, 1657–1667.
- Hong, D., Ren, G., 2011. A modeling of sliding joint on one-dimensional flexible medium. *Multibody System Dynamics* 26, 91–106.
- Kim, D., Leamy, M., Ferri, A., 2011. Dynamic Modeling and Stability Analysis of Flat Belt Drives Using an Elastic/Perfectly Plastic Friction Law. *ASME Journal of Dynamic Systems, Measurement, and Control* 133, 1–10.
- Kubas, K., 2017. A model for the dynamic analysis of a belt transmission using the Dahl friction model. *Journal of Theoretical and Applied Mechanics* 55, 1423–1435.
- Kurki, M., Jeronen, J., Saksa, T., Tuovinen, T., 2016. The origin of in-plane stresses in axially moving orthotropic continua. *International Journal of Solids and Structures* 81, 43–62.
- Leamy, M., 2005. On a Perturbation Method for the Analysis of Unsteady Belt-Drive Operation. *ASME Journal of Applied Mechanics* 72 (4), 570–580.
- Mojdehi, A., Holmes, D., Dillard, D., 2017. Friction of extensible strips: An extended shear lag model with experimental evaluation. *International Journal of Solids and Structures* 124, 125–134.

- Morimoto, T., Iizuka, H., 2012. Rolling contact between a rubber ring and rigid cylinders: Mechanics of rubber belts. *International Journal of Mechanical Sciences* 54, 234–240.
- Mote, J., 1966. On the nonlinear oscillation of an axially moving string. *Journal of Applied Mechanics* 33, 463–464.
- Pfeiffer, F., Glocker, C., 2004. *Multibody Dynamics with Unilateral Contacts*. Wiley-VCH, Weinheim.
- Reynolds, O., 1874. On the efficiency of belts or straps as communicators of work. *The Engineer* 38, 396.
- Rubin, M., 2000. An Exact Solution for Steady Motion of an Extensible Belt in Multipulley Belt Drive Systems. *Journal of Mechanical Design* 122, 311–316.
- Saksa, T., Banichuk, N., Jeronen, J., Kurki, M., Tuovinen, T., 2012. Dynamic analysis for axially moving viscoelastic panels. *International Journal of Solids and Structures* 49, 3355–3366.
- Steinbrecher, I., Humer, A., Vu-Quoc, L., 2017. On the numerical modeling of sliding beams: A comparison of different approaches. *Journal of Sound and Vibration* 408, 270–290.
- Stolarski, T. A., 1990. *Tribology in Machine Design*. Butterworth-Heinemann, Oxford.
- Vetyukov, Y., 2018. Non-material finite element modelling of large vibrations of axially moving strings and beams. *Journal of Sound and Vibration* 414, 299–317.
- Vetyukov, Y., Gruber, P., Krommer, M., 2016. Nonlinear model of an axially moving plate in a mixed Eulerian-Lagrangian framework. *Acta Mechanica* 227, 2831–2842.

- Vetyukov, Y., Gruber, P., Krommer, M., Gerstmayr, J., Gafur, I., Winter, G., 2017a. Mixed Eulerian-Lagrangian description in materials processing: deformation of a metal sheet in a rolling mill. *International Journal for Numerical Methods in Engineering* 109, 1371–1390.
- Vetyukov, Y., Oborin, E., Krommer, M., Eliseev, V., 2017b. Transient modelling of flexible belt drive dynamics using the equations of a deformable string with discontinuities. *Mathematical and Computer Modelling of Dynamical Systems* 23 (1), 40–54.
- Wetter, R., Popov, V., 2014. Shakedown limits for an oscillating, elastic rolling contact with Coulomb friction. *International Journal of Solids and Structures* 51, 930–935.
- Wickert, J., 1992. Nonlinear vibration of a traveling tensioned beam. *International Journal of Non-Linear Mechanics* 27 (3), 503–517.
- Yastrebov, V., 2013. *Numerical Methods in Contact Mechanics*. John Wiley & Sons, Ltd.